Laser-depletion spectroscopy of core-excited levels of neutral rubidium

J. K. Spong, A. Imamoğlu, R. Buffa,* and S. E. Harris
Edward L. Ginzton Laboratory, Stanford University, Stanford, California 94305
(Received 6 May 1988)

This paper describes a new technique for obtaining level positions, linewidths, autoionizing times, and oscillator strengths of core-excited levels and transitions. A tunable laser is used to deplete the population of a radiating core-excited level, as other levels within the core-excited manifold are accessed. A saturation technique which allows the measurement of autoionizing times whose linewidth lies well beneath the combined Doppler-hyperfine profile is developed and demonstrated.

I. INTRODUCTION

Core-excited levels of atoms result from the excitation of an inner-shell electron to an outer, valence orbital. These configurations generally lie above the first continuum, and so are energetically allowed to autoionize. Knowledge of the locations and lifetimes of core-excited autoionizing levels is important to the understanding of many physical processes, including dielectronic recombination, multiphoton and multielectron ionization, and harmonic generation. Because these levels can be very energetic, they may also be applicable to the construction of extreme ultraviolet (xuv) lasers.[1] Traditionally, positions of core-excited levels have been measured by either ejected electron spectroscopy[2] or xuv photoabsorption spectroscopy[3] from the ground state. These techniques in general suffer from poor resolution and are therefore incapable of measuring autoionizing lifetimes which are longer than about 1 ps. More recently, Cooke *et al.*[4] and Bloomfield *et al.*[5] have used multistep and multiphoton excitation to prepare doubly excited column II atoms and to measure their linewidths and autoionizing times.[6]

In this article we describe a new technique called depletion spectroscopy,[7–9] which allows the measurement of levels positions, linewidths, autoionizing lifetimes, and transition oscillator strengths of core-excited levels to unprecedented accuracy. Autoionizing lifetimes can be measured in the range of 10^{-9}–10^{-14} sec, including lifetimes whose Lorentz widths are far narrower than the Doppler or hyperfine width of the transition. The technique is applied to the core-excited manifold of neutral Rb. Fifteen core-excited levels are located and identified, and oscillator strengths and autoionizing lifetimes are measured. Several of these levels are found to be surprisingly stable against autoionization, and radiate strongly in the xuv on previously unobserved transitions. The wavelengths and yields of the xuv radiation support the identifications and lifetime measurements reported here.

II. DEPLETION SPECTROSCOPY OF CORE-EXCITED LEVELS

To perform depletion spectroscopy, a radiating core-excited level is used as a reference level from which to access the autoionizing manifold, as illustrated in Fig. 1. The radiating level is impulsively excited, and a detector monitors the resulting fluorescence from this level. A tunable dye laser is passed through the excited vapor to transfer the fluorescing atoms to other core-excited levels nearby. As the laser is scanned in frequency, a level is encountered, and the excited level population is transferred to it, resulting in a depletion in the amount of fluorescence observed from the reference level. The location of the depletion signal, as a function of dye laser frequency, determines the energy of the accessed level, relative to the reference level. The shape of the depleted signal, as a function of laser intensity, can be analyzed to determine the oscillator strength and Lorentz width of the transition. Because the resolving instrument is the narrow bandwidth visible dye laser, the resolution of the technique is very high.

To apply depletion spectroscopy to the core-excited manifold of an element, a radiating, core-excited level must be available to serve as the reference level. Because core-excited levels tend to autoionize rapidly, states with acceptable fluorescent yields are extremely rare. Depletion spectroscopy is made possible by the recent identification of a subclass of core-excited levels, termed

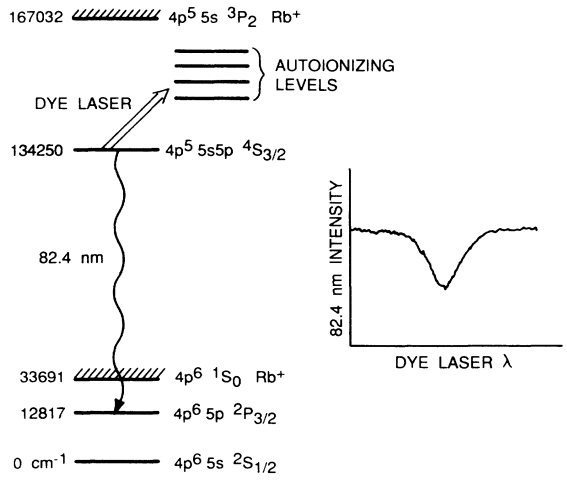

FIG. 1. Energy level diagram of Rb, showing the depletion spectroscopy technique.

"quasimetastable" levels.[10–12] Quasimetastable levels are core-excited, quartet levels that are metastable against autoionization, but radiate in the xuv to levels in the valence structure. The distinguishing feature of these quartet levels is that the spin-orbit interaction mixes the quartet eigenfunction only with doublet basis levels which are themselves forbidden to autoionize but allowed to radiate. The quasimetastable quartet levels thereby assume radiative character while retaining metastability against autoionization. Each of the column I metals and column II alkalilike ions has one or two quasimetastable levels, lying near the bottom of the core-excited manifold of each parity. Because quasimetastable levels have significant doublet admixture, and because they occur in both parities, they provide access to both doublet and quartet levels of both parities.

In rubidium, the two lowest quasimetastable levels are the odd parity $4p^5 4d5s\ ^4P_{5/2}$ and the even parity $4p^5 5s5p\ ^4S_{3/2}$. Figure 1 is a partial energy level diagram showing the location of the even parity $4p^5 5s5p\ ^4S_{3/2}$ quasimetastable level. This level lies at $134\,250.1\pm0.4$ cm^{-1} above the ground state and radiates at 82.4 nm to the $4p^6 5p^2P_{3/2}$ valence level.[13] This quasimetastable level is impulsively excited by laser-produced x-rays, and the population decays slowly by radiating at 82.4 nm. A tunable dye laser is used to detect odd parity levels with $J=\frac{1}{2}$, $\frac{3}{2}$, and $\frac{5}{2}$ by depleting the 82.4-nm fluorescence.

III. THEORETICAL DESCRIPTION OF DEPLETION SPECTROSCOPY

A. Solution of the laser-driven, two-level atomic system and the equivalent width of the depletion curve

The experimental situation, shown in Fig. 1, is well described by a two-level atomic system, where level $|1\rangle$ is the quasimetastable reference level, and level $|2\rangle$ is the autoionizing target level. Levels $|1\rangle$ and $|2\rangle$ are coupled by a laser pulse $E(t)$, via their dipole moment μ_{12}. This is the classic two-level system, except that $|1\rangle$ and $|2\rangle$ are core-excited levels which are embedded in a continuum. The interaction of level $|2\rangle$ with this continuum causes its population to autoionize at a rate Γ and its amplitude to decay at a rate $\Gamma/2$.[14] The decay of the quasimetastable level $|1\rangle$, through radiation or autoionization, is negligible on the time scale of the laser interaction. In the rotating wave approximation, the equations of motion for the level amplitudes a_1 and a_2 are

$$\frac{\partial a_1}{\partial t}=\frac{i\Omega}{2}\exp(-i\Delta t)a_2(t)\ , \tag{1a}$$

$$\frac{\partial a_2}{\partial t}=\frac{i\Omega}{2}\exp(i\Delta t)a_1(t)-\frac{\Gamma}{2}a_2(t)\ , \tag{1b}$$

where $\Omega=\mu_{12}E(t)/\hbar$ is the Rabi frequency. $\Delta=\omega_0-\omega$ is the detuning of the laser probe frequency ω from the $|1\rangle-|2\rangle$ transition frequency ω_0. For a square laser pulse and with the boundary conditions $a_1(0)=1$, $a_2(0)=0$, the solution to the coupled equations for a_1 is

$$a_1(t)=\frac{\rho_2}{\rho_2-\rho_1}\exp(\rho_1 t)-\frac{\rho_1}{\rho_2-\rho_1}\exp(\rho_2 t)\ , \tag{2}$$

where

$$\rho_{1,2}=\frac{-\Gamma/2-i\Delta}{2}\pm\frac{1}{2}\left[\frac{\Gamma^2}{4}-\Omega^2-\Delta^2+i\Gamma\Delta\right]^{1/2}\ . \tag{3}$$

In depletion spectroscopy, the fluorescence from level $|1\rangle$ (see Fig. 1) is sampled for a short time after the end of a laser pulse of length τ. This fluorescence is proportional to the atomic population remaining in level $|1\rangle$, $|a_1(\tau)|^2$. The depleted fluorescence (the difference in the fluorescence with and without the laser present) therefore has magnitude $1-|a_1(\tau)|^2$ and is given by

$$1-|a_1(\tau)|^2=1-\frac{\alpha_2^2+\beta_2^2}{(\alpha_2-\alpha_1)^2+(\beta_2-\beta_1)^2}\exp(2\alpha_1\tau)-\frac{\alpha_1^2+\beta_1^2}{(\alpha_2-\alpha_1)^2+(\beta_2-\beta_1)^2}\exp(2\alpha_2\tau)$$
$$+2\exp\left[-\frac{\Gamma}{2}\tau\right]\left[\frac{\alpha_1\alpha_2+\beta_1\beta_2}{(\alpha_2-\alpha_1)^2+(\beta_2-\beta_1)^2}\cos(\beta_2-\beta_1)\tau+\frac{\alpha_1\beta_2-\alpha_2\beta_1}{(\alpha_2-\alpha_1)^2+(\beta_2-\beta_1)^2}\sin(\beta_2-\beta_1)\tau\right]\ , \tag{4}$$

where $\alpha_{1,2}$ and $\beta_{1,2}$ are the real and imaginary parts of the eigenvalues $\rho_{1,2}$:

$$\alpha_{1,2}=\mathrm{Re}\rho_{1,2}=-\frac{\Gamma}{4}\pm\frac{1}{2}\left[\frac{\Gamma^2/4-\Omega^2-\Delta^2+[(\Gamma^2/4+\Omega^2+\Delta^2)^2-\Gamma^2\Omega^2]^{1/2}}{2}\right]^{1/2}\ , \tag{5a}$$

$$\beta_{1,2}=\mathrm{Im}\rho_{1,2}=-\frac{\Delta}{2}\pm\frac{1}{2}\left[\frac{-\Gamma^2/4+\Omega^2+\Delta^2+[(\Gamma^2/4+\Omega^2+\Delta^2)^2-\Gamma^2\Omega^2]^{1/2}}{2}\right]^{1/2}\ . \tag{5b}$$

The depleted fluorescence is monitored as a function of the laser probe frequency ω, generating a depletion curve, as indicated in Fig. 1. The experimentally measured quantity is the "equivalent width" of this curve, W_{eq}, defined as

$$W_{eq}=\int_{-\infty}^{+\infty}[1-|a_1(\tau)|^2]d\omega\ . \tag{6}$$

The equivalent width is the width of a rectangle whose area is the same as the area of the depletion curve, but whose

height is the full, undepleted signal level. The equivalent width is illustrated in Fig. 2. This quantity is also used in the curve of growth procedure[15,16] of conventional absorption spectroscopy, and the correspondence to this procedure is established in Sec. III D.

Because of the complicated form of the function $1-|a_1(\tau)|^2$, given by Eq. (4), the evaluation of the equivalent width (6) in general requires numerical computation. There is, however, a key assumption which applies to our experimental work and which greatly simplifies the calculation. This assumption is that the laser pulse length τ is long compared to the autoionizing lifetime of level $|2\rangle$, that is $\Gamma\tau \gg 1$. For this case we can write

$$W_{eq}=|2\Delta_c|+2\int_{-\infty}^{\omega_0-|\Delta_c|}[1-|a_1(\tau)|^2]d\omega \ . \tag{7}$$

The parameter Δ_c is a characteristic laser detuning such that for $|\omega_0-\omega|<|\Delta_c|$, the depletion function is saturated, i.e., $1-|a_1(\tau)|^2\rightarrow 1$. The saturated region contributes a total of $|2\Delta_c|$ to the integral. If the laser drive strength Ω is small, then the transition is never saturated, and $\Delta_c=0$. As Ω increases, the transition becomes saturated over some range of ω, and $|\Delta_c|$ increases from zero.

It is shown in the Appendix that if $\Gamma\tau \gg 1$, Eq. (7) can be written as

$$W_{eq}\approx|2\Delta_c|+2\int_{-\infty}^{\omega_0-|\Delta_c|}\left[1-\exp\left[-\frac{\Omega^2\tau}{2}\frac{\Gamma/2}{\Gamma^2/4+(\omega_0-\omega)^2}\right]\right]d\omega \ . \tag{8}$$

It is also shown in the Appendix that for $\Gamma\tau$ large, and for $|\omega_0-\omega|\leq|\Delta_c|$, the integrand in Eq. (8) is approximately unity. Therefore, we may extend the integration inside of $|\omega_0-\omega|=|\Delta_c|$ to yield

$$W_{eq}\approx\int_{-\infty}^{+\infty}\left[1-\exp\left[-\frac{\Omega^2\tau}{2}\frac{\Gamma/2}{\Gamma^2/4+(\omega_0-\omega)^2}\right]\right]d\omega \ . \tag{9}$$

The integrand in Eq. (9) is the standard rate equation solution for the transfer of population from level $|1\rangle$. This solution may be written in terms of the integrated absorption cross section σ_0 and the Lorentzian line shape $L(\omega_0-\omega)$:

$$W_{eq}\approx\int_{-\infty}^{+\infty}\{1-\exp[-I\sigma_0\tau L(\omega_0-\omega)]\}d\omega \ , \tag{10a}$$

where

$$L(\omega_0-\omega)=\frac{\Gamma/2\pi}{(\Gamma/2)^2+(\omega_0-\omega)^2}, \quad \sigma_0=\frac{\pi e^2}{2\epsilon_0 mc}f_{12} \ . \tag{10b}$$

Here, I is the laser intensity in photon/m^2/sec, f_{12} is the absorption oscillator strength, and e and m are the electron charge and mass (mks units). σ_0 has units of m^{2}rad/sec, and the Lorentzian line shape has a full width at half amplitude of Γ and is centered at ω_0.

To demonstrate the validity of the above approximation, the equivalent width (6) is evaluated using the exact expression for $1-|a_1(\tau)|^2$, given by (4), and then compared to the approximation of Eq. (9). The percent error of the approximate formula is plotted in Fig. 3 as a function of the normalized Rabi frequency Ω/Γ. Several curves are plotted in the figure, corresponding to different values of $\Gamma\tau$. In the experiment discussed in the following sections, the laser pulse length is 5 ns, and autoionizing lifetimes are generally shorter than 10^{-10} sec. Therefore, $\Gamma\tau$ is greater than 50, and, as seen from Fig. 3, the error due to the approximate form for equivalent width Eq. (9) is neglibly small.

We note that the approximations which led to Eq. (9) did not require that the Rabi frequency, Ω, be less than the autoionizing rate, Γ. Therefore, rate equations, *per se*, are not valid, and one could not have directly written Eq. (10). The essence of the simplification of Eq. (6) to Eq. (9) is as follows: In the wings of the line, the rate equation solution is valid; it is not near line center. But near line center, with the condition that $\Gamma\tau \gg 1$, the exact and the rate equation functions are both saturated. Therefore, the rate equation expression may be extended to include the full region of integration.

B. Line broadening effects

Equation (9) is the expression for the equivalent width of the depletion curve for a single atom subjected to a

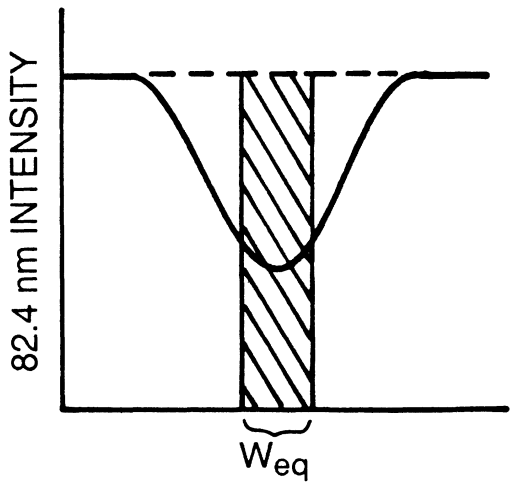

FIG. 2. The equivalent width, W_{eq}, of a depletion signal.

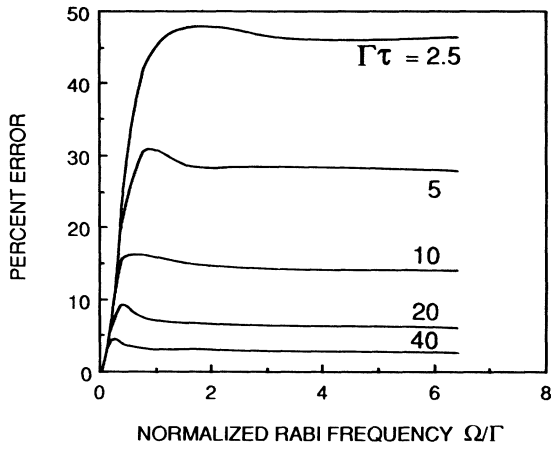

FIG. 3. Percent error in the equivalent width, W_{eq}, is plotted vs the normalized Rabi frequency, Ω/Γ, and for several values of $\Gamma\tau$.

monochromatic laser field. If, instead, the laser has a normalized Gaussian profile $G(\omega_L-\omega)$ such that $I(\omega)=I_0G(\omega_L-\omega)$, Eq. (10) becomes

$$W_{eq}=\int_{-\infty}^{+\infty}\{1-\exp[-I_0\sigma_0\tau\vartheta(\omega_0-\omega_L)]\}d\omega_L\ , \tag{11a}$$

where

$$\vartheta(\omega_0-\omega_L)=\int_{-\infty}^{+\infty}G(\omega_L-\omega)L(\omega_0-\omega)d\omega\ . \tag{11b}$$

The second integration is performed over the laser frequency components ω thereby to generate a Voigt profile $\vartheta(\omega_0-\omega_L)$.

As a result of their Doppler distribution and hyperfine structure, the atoms will also be distributed in frequency space according to a profile $D(\omega_D-\omega_0)$. The equivalent width, allowing for this distribution, as well as for the laser linewidth, becomes

$$W_{eq}=\int_{-\infty}^{+\infty}D(\omega_D-\omega_0)\times\int_{-\infty}^{+\infty}\{1-\exp[-I_0\sigma_0\tau\vartheta(\omega_0-\omega_L)]\}\times d\omega_L d\omega_0\ . \tag{12}$$

Because the range of integration over ω_L is very large compared to the convolved laser and Lorentzian linewidths, the definite integral over ω_L is independent of ω_0. We therefore take the bracketed term as a constant and integrate Eq. (12) over ω_0 to obtain

$$W_{eq}=\int_{-\infty}^{+\infty}\{1-\exp[-I_0\sigma\tau\vartheta(\omega_D-\omega_L)]\}d\omega_L\ . \tag{13}$$

After the integration we take ω_0 at its line center value ω_D. We thus obtain the important and useful result that the equivalent width is independent of the atomic Doppler and hyperfine distribution. It does depend on the (measurable) laser linewidth and, of course, on the Lorentzian linewidth.

C. Measurement of Lorentz widths and oscillator strengths

In general, curve fitting techniques must be used to deconvolve the Lorentzian and laser linewidths in Eq. (13). The procedure is to integrate numerically Eq. (13) to obtain W_{eq} as a function of $I_0\sigma_0\tau$, with the Lorentzian and laser linewidths as parameters. Using the measured values of laser linewidth, I_0, and τ, the integrated cross section σ_0 and the Lorentz width Γ are adjusted to achieve a best fit between the experimental and calculated curves. This technique is in one-to-one correspondence with the "curve of growth" method which is used in absorption spectroscopy, and this analogy will be discussed further in the next section.

There is, however, a simple analytical form for Eq. (13) in either of two limits: a laser energy density, which is low compared to the transition saturation energy $1/[\sigma_0\vartheta(0)]$, or a laser energy which is high compared to the saturation energy.

If $I_0\sigma_0\tau\vartheta(0)\ll 1$, series expansion of Eq. (13) yields

$$W_{low}=\int_{-\infty}^{+\infty}I_0\sigma_0\tau\vartheta(\omega_0-\omega_L)d\omega_L =I_0\sigma_0\tau\ . \tag{14}$$

Here, the equivalent width does not depend on any broadening mechanisms, but only on the laser energy and the integrated cross section. Since the integrated cross section is related to the transition oscillator strength f_{12} by Eq. (10b), Eq. (14) allows the determination of the oscillator strength of the transition.

If one increases the laser energy by a factor κ, such that $\kappa I_0\sigma_0\tau\vartheta(0)\gg 1$, the high-energy equivalent width approximates the equivalent width of a Lorentzian line shape and may be shown[15] to be given by

$$W_{high}=(2\kappa I_0\sigma_0\tau\Gamma)^{1/2}\ . \tag{15}$$

Combining Eqs. (14) and (15), the Lorentzian linewidth is

$$\Gamma=\frac{(W_{high})^2}{2\kappa W_{low}}\ . \tag{16}$$

Equation (16) allows the determination of the Lorentzian linewidth, and thus the autoionizing time, by measuring only the ratio of laser energy densities in the two regimes. It does not require knowledge of the transition oscillator strength, absolute pulse energy, or laser line shape. The ratio method is applicable when one can achieve high-energy equivalent widths such that $W_{high}/\delta\omega_L \gg \delta\omega_L/\Gamma$, where $\delta\omega_L$ is the laser linewidth. If insufficient laser energy is available to strongly saturate weaker transitions, a full curve of growth treatment is necessary.

D. Correspondence to the curve of growth procedure in laser absorption spectroscopy

In the curve of growth procedure, as used in absorption spectroscopy, a laser is passed through a sample of N atoms per cm^3 of length l, and the absorption of the laser is measured as a function of its frequency. The area of

the absorption versus frequency plot, i.e., the equivalent width, is given by[15,16]

$$W_{\text{eq,absorption}} = \int_{-\infty}^{+\infty} \{1-\exp[-N\sigma_0 l V(\omega_D-\omega_L)]\} d\omega_L \ . \quad (17)$$

Here $V(\omega_D-\omega_L)$ is the Voigt profile of the convolved Lorentzian and Doppler linewidths, i.e.,

$$V(\omega_D-\omega_L)=\int D(\omega_D-\omega_0)L(\omega_0-\omega_L)d\omega_0 \ . \quad (18)$$

Comparison of the equivalent width of absorption spectroscopy [Eqs. (17) and (18)] with that of depletion spectroscopy [Eqs. (13) and (11b)] shows that there is a one-to-one correspondence between the variables:

$$\begin{aligned} &Nl \leftrightarrow I_0\tau \ , \\ &D(\omega_D-\omega_0)\leftrightarrow G(\omega_L-\omega) \ . \end{aligned} \quad (19)$$

Thus atoms per cm^2 in absorption spectroscopy become photons per cm^2 in depletion spectroscopy, and correspondingly the Doppler linewidth of absorption spectroscopy goes to the laser linewidth of depletion spectroscopy. The equivalent width in absorption spectroscopy is invariant to the laser linewidth, and the equivalent width in depletion spectroscopy is invariant to the Doppler linewidth. Thus the numerical integration routines[15,16] developed for curve of growth absorption spectroscopy may be used to analyze depletion spectroscopy. We note that this correspondence only holds for depletion spectroscopy in the limit of long $\Gamma\tau$.

IV. EXPERIMENTAL APPARATUS: EXCITATION OF QUASIMETASTABLE LEVELS WITH LASER-PRODUCED X-RAYS

In the experiment described here, the Rb $4p^5 5s 5p\ ^4S_{3/2}$ quasimetastable level is impulsively excited by a flash of soft x rays from a laser-produced plasma. The experimental apparatus of the laser-produced plasma source is shown schematically in Fig. 4. A 150 mJ, 7-ns pulse of 1064-nm radiation is focused onto a solid, rotating tantalum target, forming a laser plasma at the site. The plasma emits a blackbodylike continuum of soft x rays which efficiently overlaps the p-shell photoionization cross section of Rb. Photoionization of ground-state Rb results in large densities of ions in the excited configuration $Rb^+ 4p^5 5s$, distributed among the available $^1P_1$ and $^3P_{0,1,2}$ levels. The $Rb^+ 4p^5 5s\ ^3P_1$ ion level lies 134 869 cm^{-1} above the ground state of the ion,[17] and only 619 cm^{-1} away from the absolute energy of the Rb quasimetastable level at 134 250 cm^{-1}. The ion level undergoes near-resonant charge transfer collisions with the ground-level neutral atoms, according to

$$Rb^+ 4p^5 5s\ ^3P_1 + Rb\, 4p^6 5s\ ^2S_{1/2} \rightarrow Rb^+ 4p^6\ ^1S_0 + Rb^* 4p^5 5s 5p\ ^4S_{3/2} + 619 \text{ cm}^{-1} \quad (20)$$

forming quasimetastable atoms and ground level ions. Quasimetasable densities on the order of 1×10^{12} cm^{-3} are created via this charge transfer mechanism.[18] The quasimetastable atoms then decay by radiating at 82.4 nm, and the radiation is collected by a low-resolution spectrometer.

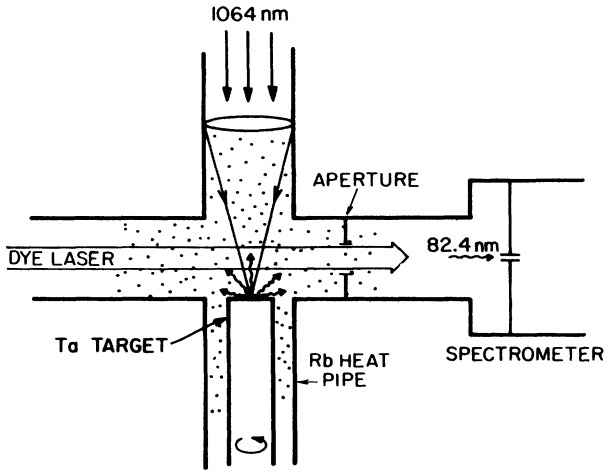

FIG. 4. Schematic of the experimental apparatus.

Rb vapor at a density of 2×10^{16} cm^{-3} is provided by heating a reservoir of Rb liquid to 300 °C. The Rb metal is contained in a T-shaped stainless-steel cell as shown in Fig. 4. The metal vapor is confined to the center of the cell by operating the cell in a heat pipe mode, with 1 torr of neon, introduced at the ends of the cell arms, serving as the buffer gas. A low-resolution 0.2-m Acton vacuum spectrometer views the vapor through a limiting aperture. The aperture serves to shield the spectrometer from the broadband laser plasma light and to restrict its view to the path of the transfer dye laser. The spectrometer was equipped with a Galileo chevron microchannel plate (MCP) detector, operated at 2500 V. This detector has a relatively fast, 1-ns response time, and excellent rejection of visible dye laser photons. Signal from the MCP went to a gated integrator, whose output was digitized and

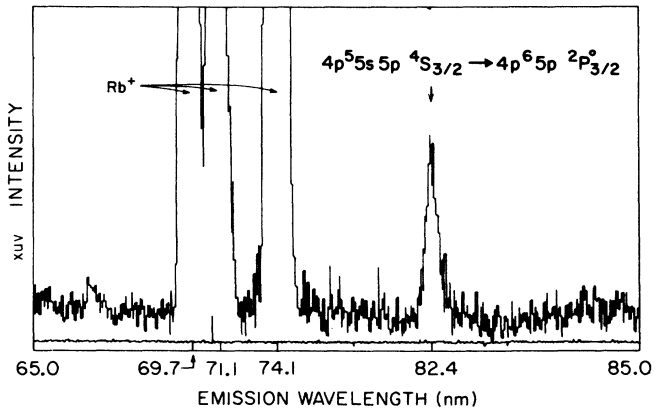

FIG. 5. xuv emission spectrum of Rb.

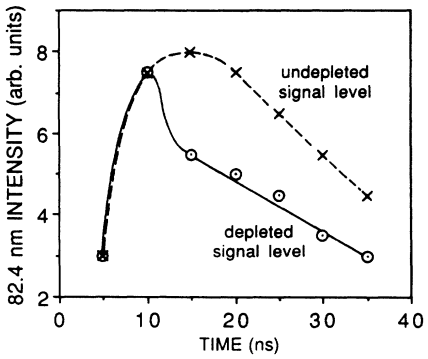

FIG. 6. 82.4 nm intensity as a function of time, showing the slow recovery of the depleted signal level relative to the undepleted signal level.

averaged by a computer. The computer also controlled the dye laser tuning.

The transfer beam is the output of a dye laser pumped by the same Nd:YAG laser (where YAG stands for yttrium aluminum garnet) which provided the 1064-nm beam. The dye laser traverses the excited Rb vapor along the line of sight of the spectrometer, as shown in Fig. 4, and is delayed 20 ns relative to the 1064-nm beam. The beam passes through the limiting aperture, transferring population in the region viewed by the spectrometer. The dye laser is grating tuned, resulting in a bandwidth of about 0.4 cm^{-1}, and has a pulse duration of 5 ns. The 10-ns detector gate is placed immediately after the end of the dye laser pulse. No external timing of the pump and transfer beams is required since they are generated by the same laser, and separated in time by an optical delay.

Because xuv detectors must be evacuated, a pressure barrier must be placed between the MCP detector and the Rb vapor cell to separate the two pressure regions. A microchannel plate, or capillary array, is placed at the entrance to the xuv spectrometer to provide this barrier. The plate is a 500-μm-thick quartz window through which channels of diameter 50 μm have been drilled. The channels are so numerous that the window is 50% open area. The capillary array therefore transmitted $\sim$50% of the xuv photon flux while having poor enough gas conductance to allow differential pumping of the system. The turbopump supplied with the xuv spectrometer was sufficient to maintain a 10^{-4}-torr vacuum in the spectrometer and detector, while the heat pipe cell was run at 1 torr. By providing a buffer gas inlet directly in front of the capillary array, the system could be differentially pumped without disturbing the Rb heat pipe.

Figure 5 shows an emission scan of soft-x-ray excited Rb vapor, taken 20 ns after the 1064-nm laser pulse. Because p-shell photoionization is the pumping mechanism, no higher ionization species are excited, so that the xuv spectrum consists only of Rb II lines at 69.7, 71.1, and 74.1 nm and the quasimetastable emission at 82.4 nm. Over a 10-nm-wide spectral region, the 82.4-nm quasimetastable radiation is the dominant spectral feature. This allows use of 1-mm-wide spectrometer slits and therefore relatively good collection efficiency. Laser-produced x-ray excitation generated about 10 detected counts on the 82.4-nm emission line in a 5-ns gate in a 5-mm diameter aperture. This large count rate allowed analog detection with a good signal-to-noise ratio. Large signals also made rapid data collection possible; the dye laser was typically scanned at 1 cm^{-1}/sec. This rate is sufficient to scan a typical dye range in about 20 min, and cover the visible spectrum in about 4 h.

An important feature of laser-produced x-ray excitation is that it occurs on a time scale which is short compared to the lifetime of the quasimetastable level. The level is pumped for only about 15 ns, which is the duration of the ion population created by the 7-ns laser-produced plasma. Verification of the impulsive nature of the soft-x-ray excitation was provided by depleting the

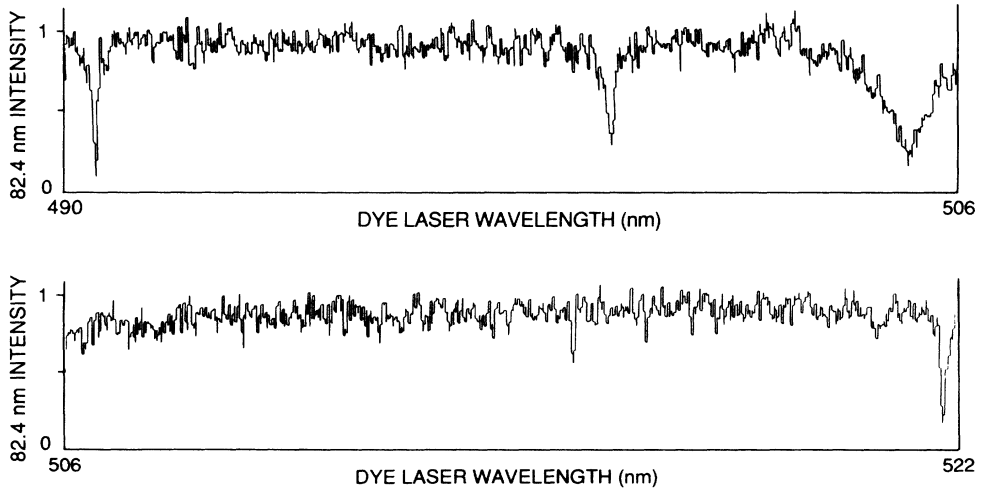

FIG. 7. Depletion scan of the tuning range 490–522 nm.

quasimetastable level after excitation, and measuring the recovery of the population. Figure 6 shows the quasimetastable fluorescence level as a function of time. The upper curve shows the undepleted signal level; for the lower curve, the quasimetastable fluorescence was reduced by about 30% by the transfer laser. As can be seen in the figure, the depletion of the fluorescence persists more than 20 ns after the passage of the 5-ns dye laser pulse. On the time scale of the 10-ns data gates used, the excitation rate into the quasimetastable level is therefore negligible. Transfer of the population out of the quasimetastable level can then take place after excitation has ceased. This feature gives good contrast to the depletion signals, and makes the curve of growth treatment outlined in the preceding section applicable to depletion spectroscopy when performed with this excitation method.

V. DEPLETION SPECTRA AND RESULTS

A. Experimental data and analysis

Figure 7 shows the signal level at 82.4 nm as a function of dye laser wavelength for the tuning range of Coumarin 500. The scan covers a 1300-cm^{-1}-wide spectral region and requires 20 min of data collection. The contrast achieved in the depletion signals is about 80%. Failure of the depleted signal to reach the baseline is attributed to imperfect overlap of depleted and viewed volumes and some repumping of the depleted level. An 80% reduction of fluorescence from the quasimetastable level was the maximum we were able to achieve, and equivalent widths are measured relative to this baseline.

Four depletion signals are evident in this scan; they are positioned at 490.5, 499.8, 505.1, and 521.7 nm of the transfer laser wavelength. In absolute energy[13] these levels therefore lie at 154 631, 154 253, 154 044, and 153 412 cm^{-1}, respectively. Two of these levels, those at 154 044 cm^{-1} and 154 253 cm^{-1}, have been previously seen in photoabsorption spectroscopy,[3] and the level at 153 412 cm^{-1} has been observed in ejected electron spectroscopy.[2] The remaining feature in this scan, at 154 631 cm^{-1} has not been previously observed.

The very wide feature at 154 044 cm^{-1}, slightly saturated in Fig. 7, has an autoionizing lifetime so short that its large natural linewidth dominates other broadening mechanisms. For such cases, if the transition is not saturated, the full width of the depletion scan is the Lorentz width of the level, and the reciprocal of this width (in units of radians per second) is the autoionizing lifetime. For this level, measured at a sufficiently low laser energy so that there is no saturation, the full width is 33 cm^{-1} and corresponds to an autoionizing time of 0.16 ps.

For narrower features, the equivalent width method described in Sec. III must be employed. This method is demonstrated in Figs. 8(a), 8(b), and 8(c), which show the depletion signal located at 451.7 nm, accessing a level at 156 384 cm^{-1}. The dashed line in each figure is a computer generated curve, which has an equivalent width matching the experimental measurement. The laser energy, E/A in J/cm^2, is given for each curve ($E/A = \hbar\omega I_0 \tau \times 10^{-4}$). At low probe laser energies [Fig. 8(a)], the depletion signal is exceedingly narrow, with a halfwidth under 1 cm^{-1}. At higher laser energies, the depletion shape becomes deeper, as in Fig. 8(b), until it saturates and broadens, as shown in Fig. 8(c).

Comparing Figs. 8(a), 8(b), and 8(c), the equivalent width of the depletion signal is observed to increase from 0.61 to 3.8 cm^{-1}, when the laser energy is increased by a factor of 35. According to Eq. (13), the Lorentz width of this level is therefore 0.31 cm^{-1}. A curve of growth fit to this data gives the transition a Lorentz width of 0.29 cm^{-1} and an oscillator strength ($g_1 f_{12}$) of 0.01.

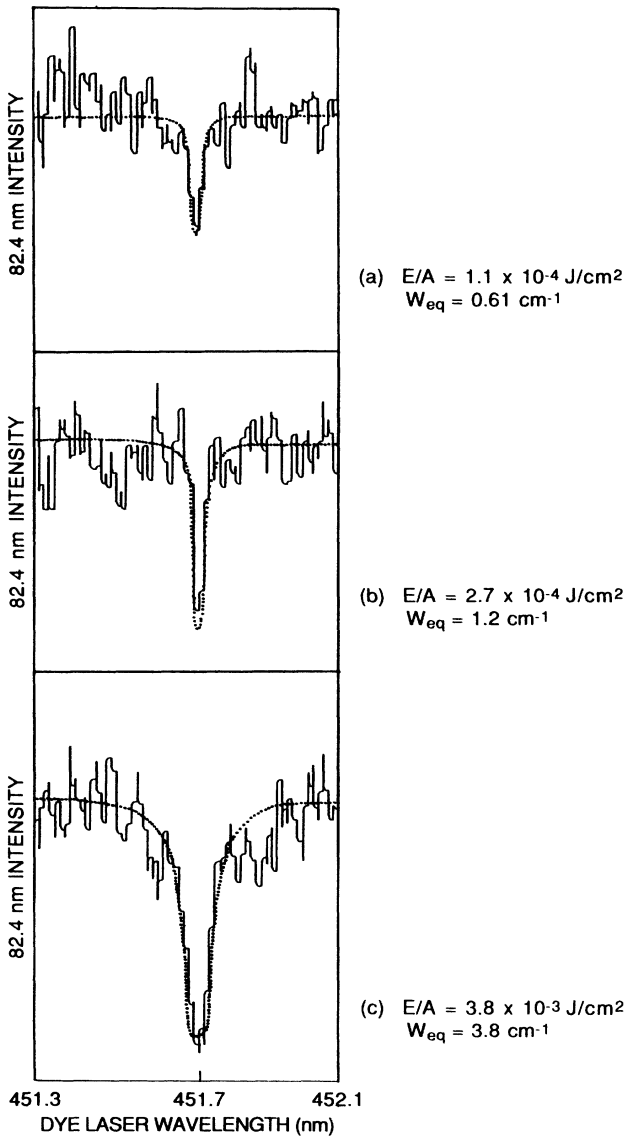

FIG. 8. Curve of growth technique applied to a depletion feature at 451.7 nm. The laser linewidth for this figure is 0.6 cm^{-1}.

TABLE I. Summary of experimental results: Transition wavelengths, low- and high-energy equivalent widths, transition oscillator strengths, and Lorentz widths. The laser probe width for these measurements was about 0.5 cm^{-1}.

λ[a] (nm)	$(E/A)_{low}$ (J/cm^2)	W_{low} (cm^{-1})	$(E/A)_{high}$ (J/cm^2)	W_{high} (cm^{-1})	$g_1 f_{12}$[b]	Lorentz width[c] (cm^{-1})
682.28	2.9×10^{-4}	0.56	2.3×10^{-3}	1.5	0.003	0.26
611.93	1.2×10^{-6}	0.50	6.0×10^{-4}	8.0	0.7	0.13
585.99	6.8×10^{-6}	0.49	3.4×10^{-4}	1.1	0.2	<0.010
553.40	3.6×10^{-5}	0.60	3.6×10^{-3}	2.2	0.05	0.017
521.72	1.6×10^{-5}	0.54	5.7×10^{-4}	3.3	0.07	0.29
505.06	1.0×10^{-3}	28			0.1	33
499.80	3.3×10^{-3}	7.7			0.006	4.8
490.52	1.4×10^{-4}	0.93	1.9×10^{-3}	4.1	0.02	0.48
482.96	1.5×10^{-4}	4.4			0.08	7.4
476.72	5.7×10^{-5}	1.1	2.0×10^{-3}	9.2	0.05	1.1
454.83	1.2×10^{-4}	0.76	1.8×10^{-3}	2.7	0.02	0.24
453.75	3.2×10^{-3}	3.8			0.003	3.5
453.03	7.0×10^{-5}	0.97	1.0×10^{-3}	6.4	0.04	1.4
451.67	1.1×10^{-4}	0.61	3.8×10^{-3}	3.8	0.01	0.29
425.55	1.2×10^{-3}	4.9			0.008	5.2

[a]Accurate to about ±0.03 nm.
[b]Accurate to a factor of 2.
[c]Accurate to a factor of 0.5.

B. Results and discussion

Tables I and II summarize the data that we have collected on the core-excited levels of neutral Rb. Table I lists 15 core-excited transitions located by scanning a dye laser from 700 nm (14 300 cm^{-1}) to 400 nm (25 000 cm^{-1}). Listed with each transition are their low- and high-energy equivalent widths, and low- and high-energy densities. High-energy equivalent widths are not given for lines which are wide enough to be measured directly from the depletion curve. The sixth and seventh columns are the transition oscillator strengths and Lorentz widths which are obtained from this data.

Table II lists the absolute energy levels accessed in each of the 15 transitions, the level designation given to each, and its autoionizing time. The absolute energies are based on the placement of $4p^5 5s 5p\ ^4S_{3/2}$ by Reader[13] at $134\,250.1\pm0.4$ cm^{-1}. The autoionizing time t is related to the Lorentz width given in Table I by $t = (2\pi c \times \text{Lorentz width})^{-1}$. This assumes that the mea-

TABLE II. Measured energy levels and tentative identifications. Energies and autoionizing lifetimes are compared to RCN/RCG calculations.

Absolute energy (expt.)[a] (cm^{-1})	Tentative designation	Absolute energy (code) (cm^{-1})	Autoionizing time (expt.)[b] (ps)	Autoionizing time (code) (ps)
148 902.7	$4p^5 4d\,(^3D)5s\ ^2D_{3/2}$	148 050	20	17
150 587.2	$4p^5 5s 6s\ ^4P_{5/2}$	150 787	41	4700
151 310.4	$4p^5 5s 6s\ ^4P_{3/2}$	151 412	>500	19
152 315.0	$4p^5 5s 6s\ ^2P_{1/2}$	152 144	310	450
153 412.0	$4p^5 5p^2(^3P)\ ^4P_{5/2}$	153 162	18	4400
154 044.0	$4p^5 5p^2(^3P)\ ^4P_{3/2}$	152 561	0.16	0.15
154 252.5	$4p^5 4d(^1P)5s\ ^2P_{3/2}$	154 514	1.1	0.05
154 630.8	$4p^5 5p^2(^3P)\ ^4D_{5/2}$	154 763	11	2500
154 950.2	$4p^5 5p^2(^3P)\ ^4P_{1/2}$	154 892	0.72	0.13
155 221.0	$4p^5 4d^2(^3F)\ ^4D_{3/2}$	155 239	4.8	9.7
156.230.1	$4p^5 4d^2(^3F)\ ^4D_{1/2}$	155 620	22	0.68
156 282.4	$4p^5 5s\,(^3P)5d\ ^2P_{3/2}$	156 191	1.5	0.07
156 317.4	$4p^5 4d^2(^1D)\ ^2P_{1/2}$	156 363	3.8	0.13
156 383.8	$4p^5 5s\,(^3P)5d\ ^4D_{5/2}$	156 990	18	20
157 742.8	$4p^5 5s\,(^3P)5d\ ^2D_{3/2}$	157 049	1.0	12

[a]The total level energies are based on the Reader (Ref. 13) value of $134\,250.0\pm0.4$ cm^{-1} for the $4p^5 5s 5p\ ^4S_{3/2}$, level, and are accurate to about ±1 cm.
[b]Accurate to about a factor of 0.5.

sured Lorentz width is determined strictly by autoionization. This is valid for all levels except $4p^5 5s 6s\ ^4P_{3/2}$ and $4p^5 5s 6s\ ^2P_{1/2}$, where the widths include a substantial radiative component. For narrow lines, the level positions have an accuracy of about 1 cm^{-1}, with this uncertainty due to the probe linewidth and calibration. Lifetimes and Lorentz widths are accurate to about 50%, mainly due to the uncertainty in the unsaturated equivalent widths. Oscillator strength measurements have an uncertainty of a factor of 2, in part due to equivalent width measurement and in part from the uncertainty in the measurement of the laser pulse energy.

The autoionizing lifetime measurements in Table II span nearly 4 orders of magnitude. For the level at 151 310 cm^{-1} we measure a lifetime of 2.5 ns. But since this lifetime does not satisfy the condition $\Gamma\tau \gg 1$, the measurement is subject to greater uncertainty, and we bound the lifetime at > 500 ps.

The identifications in Table II are made by comparing the experimental positions, lifetimes and oscillator strengths with the results of a multiconfiguration Hartree-Fock calculation, performed by the RCN/RCG atomic physics code.[19] The code runs were made including the $4p^5 5s^2$, $4p^5 5s 6s$, $4p^5 5s 7s$, $4p^5 4s 5s$, $4p^5 5d 5s$, $4p^5 5p^2$, and $4p^5 4d^2$ configurations with a scale factor of 0.77 for all radial integrals. The results of this computation are included in Table II, which lists the RCN/RCG calculated energies and autoionizing times for each level.

For many of the levels listed in Table II, identifications have been made previously,[20] based on photoabsorption and ejected electron spectroscopy data. The level identifications given here disagree in every case with these assignments. Level No. 2, at 150 587 cm^{-1}, has been seen in ejected electron spectroscopy and identified as the even parity $4p^5 5s 5p\ ^2D_{3/2}$ level. Our ability to access it, with large transition oscillator strength, from the $4p^5 5s 5p\ ^4S_{3/2}$ quasimetastable level, instead identifies the level as having odd parity. The identification given this level in Table II is $4p^5 5s 6s\ ^4P_{5/2}$. This is consistent with the failure to observe this level in absorption spectrosco-

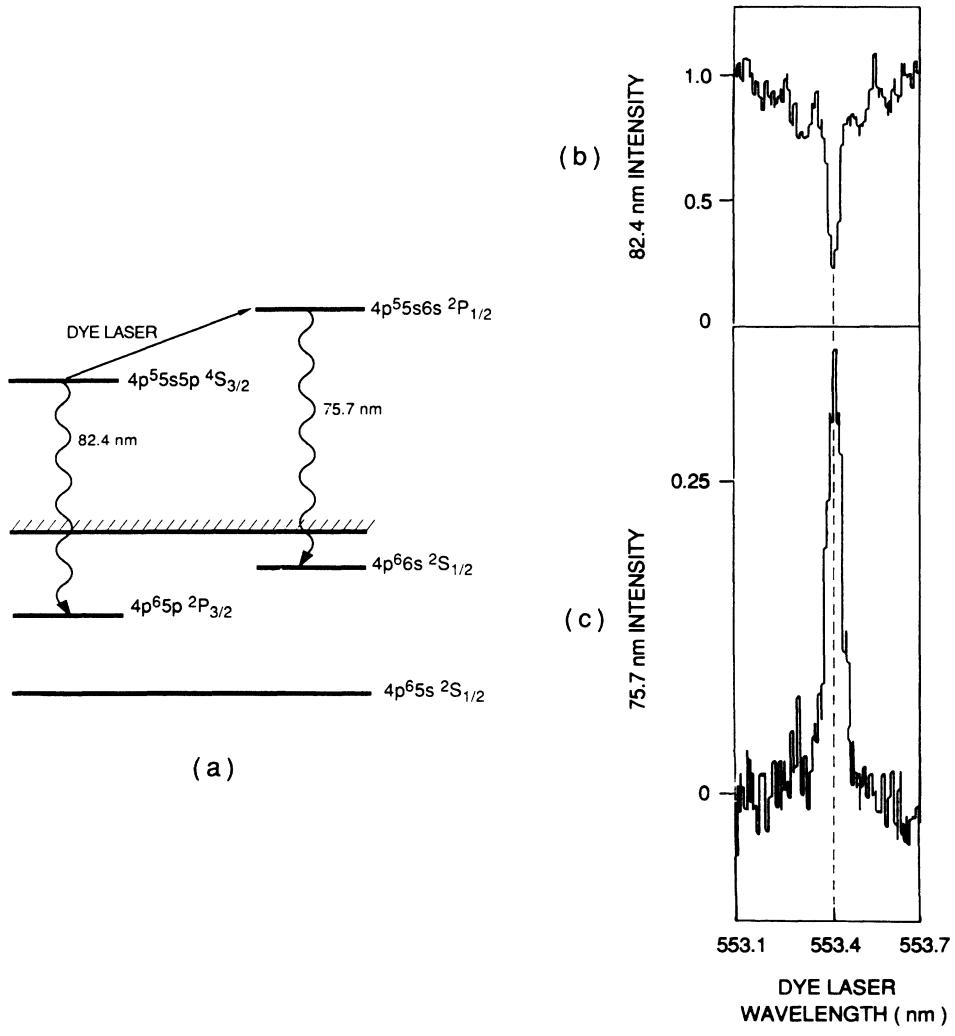

FIG. 9. (a) Energy level diagram showing the laser-induced fluorescence technique. (b) Depletion of 82.4-nm fluorescence by dye laser transfer at 553.4 nm. (c) Laser-induced fluorescence at 75.7 nm.

py from the ground state. As discussed in the next section, laser-induced xuv fluorescence was detected from three of the longer-lived levels, No. 1, No. 3, and No. 4. The wavelength of the fluorescence verified the configuration identification for these levels. This evidence, in conjunction with the RCN/RCG code calculations, strongly supports the designations given here.

By comparing experimental data to the calculated predictions in Table II, some generalizations can be made on the ability of the RCN/RCG computer code to predict level positions and autoionizing times. In 14 of 15 cases, predicted energy levels are within 700 cm^{-1}, or 0.5%, of the absolute energy of the experimental levels with which they were identified. Autoionization times generally agree to within a factor of 5, though the absolute numbers range over 4 orders of magnitude. Large discrepancies in the autoionizing times are noted for three $J=\frac{5}{2}$ levels, $4p^5 5s 6s\ ^4P_{5/2}$, $4p^5 5p^2\ ^2P_{5/2}$, and $4p^5 p^2\ ^4D_{5/2}$, which have predicted lifetimes of several nanoseconds. Lifetimes calculations are difficult for such levels, which autoionize through small or second-order mixings with doublets.

C. Extreme ultraviolet fluorescence from Rb autoionizing levels

Lifetime measurements performed on these core-excited levels indicate that several are stable enough against autoionization to have significant branching ratios to radiation in the xuv. In the experiment described below, laser-induced fluorescence is used to observe the radiative decay of these levels to levels in the valence manifold, and to estimate their radiative branching ratios.

As in depletion spectroscopy, a tunable dye laser is used to transfer the quasimetastable population to core-excited levels listed in Table II, as shown in Fig. 9(a). The transfer of population results not only in a depletion of fluorescence from the quasimetastable level, but also, in some cases, the appearance of laser-induced fluorescence from the accessed level. When laser-induced fluorescence is observed, the wavelength of the xuv radiation is measured. Subtracting this transition energy from the upper level energy listed in Table II identifies the valence level to which the core-excited atom has radiated. The radiative branching ratio of the autoionizing level can be estimated, based on the magnitude of the laser-induced fluorescence, relative to the depleted signal level. This procedure and the raw data can be found elsewhere.[18,21]

Figures 9(b) and 9(c) show the results of the laser-induced fluorescence technique applied to the core-excited transition at 553.4 nm. This wavelength is identified in Table I as belonging to the $4p^5 5s 5p\ ^4S_{3/2} \rightarrow 4p^5 5s 6s\ ^2P_{1/2}$ transition. The upper level, $4p^5 5s 6s\ ^2P_{1/2}$, lies 152 315 cm^{-1} above ground. Figure 9(b) shows the 82.4-nm quasimetastable intensity as a function of dye laser wavelength as the laser is tuned through this transition. At line center of the transition, an 80% depletion of the 82.4-nm quasimetastable fluorescence level is observed. In Fig. 9(c), the spectrometer is tuned to 75.7 nm, and the signal level is recorded as a function of dye laser wavelength. At line center of the transfer transition, laser-induced fluorescence is observed. The wavelength of the induced fluorescence, 75.7 nm, corresponds to a transition energy of 132 100 cm^{-1}, and identifies the lower level as $4p^6 6s\ ^2S_{1/2}$. The xuv transition at 75.7 nm is therefore identified as $4p^5 5s 6s\ ^2P_{1/2} \rightarrow 4p^6 6s\ ^2S_{1/2}$.

Laser-induced fluorescence was detected from the core-excited levels $4p^5 4d 5s\ ^2D_{3/2}$, $4p^5 5s 6s\ ^4P_{3/2}$, and $4p^5 5s 6s\ ^2P_{1/2}$. These levels were observed to radiate at 77.2, 76.0, and 75.7 nm, respectively, on transitions of the type $4p^5 5snl \rightarrow 4p^6 nl$. Their branching ratios to radiation are estimated as 0.02, 0.7, and 0.2, respectively. In each case, the wavelength of the transition and the radiative branching ratio support the identification and lifetime measurements of Table II. No emission was observed from the remaining 12 core-excited levels.

VI. SUMMARY

The paper develops and demonstrates the methodology of the new technique of depletion spectroscopy. The technique allows the measurement of energy level positions, transition oscillator strengths, linewidths, and autoionizing lifetimes of core-excited levels, all to unprecedented accuracy. A saturation technique which allows the measurement of autoionizing times of levels which are so long that their linewidths lie well beneath their Doppler profiles is demonstrated. It is shown that this technique does not require knowledge of the inhomogeneous broadening of the transition. A duality with the curve of growth technique of absorption spectroscopy is developed. Fifteen transitions in neutral Rb are studied, and experimental results are compared to RCN/RCG calculations.[19] In each instance, level identifications are found to be in disagreement with those given previously.

ACKNOWLEDGMENTS

The authors greatly appreciate the contributions of J. D. Kmetec and J. F. Young, and thank Joseph Reader for his measurement of the absolute energy of the $4p^5 5s 5p\ ^4S_{3/2}$ level. The work described here was supported by the U.S. Air Force Office of Scientific Research and the U.S. Army Research Office.

APPENDIX

It is shown here that Eq. (6) may be approximated by Eq. (9). We assume a laser detuning Δ such that $|\Delta|$ is greater than $|\Delta_c|$, which is itself much greater than the Rabi frequency, Ω. The square roots in the expressions for $\alpha_{1,2}$ and $\beta_{1,2}$ can be expanded in a binomial series, in powers of

$$\Gamma^2\Omega^2/(\Gamma^2/4+\Omega^2+\Delta^2)^2 \approx \Gamma^2\Omega^2/(\Gamma^2/4+\Delta^2)^2 .$$

Since $|\Delta| \gg \Omega$, it is valid to keep only the first term of the expansion; $\alpha_{1,2}$ and $\beta_{1,2}$ are then given by

$$\alpha_{1,2} \approx -\frac{\Gamma}{4} \pm \frac{\Gamma}{4} \mp \frac{\Gamma\Omega^2}{8(\Gamma^2/4+\Delta^2)} , \tag{A1a}$$

$$\beta_{1,2} \approx -\frac{\Delta}{2} \pm \frac{\Delta}{2} \mp \frac{\Gamma^2/4}{4(\Gamma^2/4+\Delta^2)} \frac{\Omega^2}{\Delta} . \tag{A1b}$$

Noting that $\alpha_2 \approx -\Gamma/2$, $|\alpha_2| \gg |\alpha_1|$, and $\beta_2 \approx -\Delta$, $|\beta_2| \gg |\beta_1|$, Eq. (4) can now be written

$$1-|a_1(\tau)|^2 \approx 1-\exp\left[-\frac{\Omega^2\tau}{2}\frac{\Gamma/2}{(\Gamma^2/4+\Delta^2)}\right]-\frac{\alpha_1^2+\beta_1^2}{\alpha_2^2+\beta_2^2}\exp(-\Gamma\tau)$$
$$+2\exp\left[-\frac{\Gamma\tau}{2}\right]\left[\frac{\alpha_1\alpha_2+\beta_1\beta_2}{\alpha_2^2+\beta_2^2}\cos(\beta_2-\beta_1)\tau\frac{\alpha_1\beta_2-\alpha_2\beta_1}{\alpha_2^2+\beta_2^2}\sin(\beta_2-\beta_1)\tau\right] . \tag{A2}$$

If $\Gamma\tau \gg 1$, then $\exp(-\Gamma\tau) \to 0$, and the exact solution reduces to

$$1-|a_1(\tau)|^2 \approx 1-\exp\left[-\frac{\Omega^2\tau}{2}\frac{\Gamma/2}{(\Gamma^2/4+\Delta^2)}\right] . \tag{A3}$$

For a given value of Δ_c, there exists a value $\Gamma\tau \gg 1$ such that

$$\left[\frac{\Omega^2}{4(\Gamma^2/4+\Delta_c^2)}\right]\Gamma\tau \gg 1 \tag{A4}$$

and so for $|\Delta| \leq |\Delta_c|$, the depletion function (A3) is saturated $[1-|a_1(\tau)|^2 \approx 1]$. Therefore, for $\Gamma\tau \gg 1$, Eq. (6) can be approximated by Eq. (9). The accuracy of the approximation is examined numerically in Fig. 3.

*Present address: Dipartimento di Fisica Universita' di Firenze, 50125 Firenze, Italy.

[1]S. E. Harris and J. F. Young, J. Opt. Soc. Am. **4**, 547 (1987).
[2]V. Pejčev, D. Rassi, K. J. Ross, and T. W. Ottley, J. Phys. B **10**, 1653 (1977).
[3]M. W. D. Mansfield, Astrophys. J. **183**, 691 (1973).
[4]W. E. Cooke, T. F. Gallagher, S. A. Edelstein, and R. M. Hill, Phys. Rev. Lett. **40**, 178 (1978).
[5]L. A. Bloomfield, R. R. Freeman, W. E. Cooke, and J. Bokor, Phys. Rev. Lett. **53**, 2234 (1984).
[6]W. E. Cooke, S. A. Bhatti, and C. L. Cromer, Opt. Lett. **7**, 69 (1982).
[7]J. K. Spong, J. D. Kmetec, S. C. Wallace, J. F. Young, and S. E. Harris, Phys. Rev. Lett. **58**, 2631 (1987).
[8]S. E. Harris, J. F. Young, A. J. Mendelsohn, D. E. Holmgren, K. D. Pedrotti, and D. P. Dimiduk, in *Laser Spectroscopy VII*, edited by T. W. Hänsch and Y. R. Shen (Springer-Verlag, New York, 1985), pp. 162–165.
[9]K. D. Pedrotti, Opt. Commun. **62**, 250 (1987).
[10]S. E. Harris, D. J. Walker, R. G. Caro, A. J. Mendelsohn, and R. D. Cowan, Opt. Lett. **9**, 168 (1984).
[11]A. J. Mendelsohn, C. P. J. Barty, M. H. Sher, J. F. Young, and S. E. Harris, Phys. Rev. A **35**, 2095 (1987).
[12]D. P. Dimiduk, Ph.D. dissertation, Stanford University, 1986.
[13]Joseph Reader, Phys. Rev. A **36**, 415 (1987).
[14]Claude Cohen-Tannoudji, Bernard Diu, and Franck Laloe *Quantum Mechanics* (Hermann, Paris, France, 1977), Vol. II, pp. 1343–1347.
[15]S. S. Penner, *Quantitative Molecular Spectroscopy and Gas Emissivities* (Addison-Wesley, Reading, MA, 1959), pp. 44–59.
[16]Anne P. Thorne, *Spectrophysics* (Chapman and Hall, London, 1974), pp. 307–311.
[17]Joseph Reader and Gabriel Epstein, J. Opt. Soc. Am. **63**, 1153 (1973).
[18]J. K. Spong (unpublished).
[19]Robert D. Cowan, *The Theory of Atomic Structure and Spectra* (University of California Press, Berkeley, California, 1981), Secs. 8-1, 16-1, and 18-7.
[20]M. W. D. Mansfield, Proc. R. Soc. London, Ser. A **364**, 135 (1978).
[21]J. K. Spong, A. Imamoğlu, J. D. Kmetec, and S. E. Harris (unpublished).